THE ASTROPHYSICAL JOURNAL, 252:10–31, 1982 January 1

A HIGH-RESOLUTION STUDY OF THE ABSORPTION SPECTRA OF THREE QSOs: EVIDENCE FOR COSMOLOGICAL EVOLUTION IN THE LYMAN-ALPHA LINES

PETER YOUNG[1] AND WALLACE L. W. SARGENT
Palomar Observatory, California Institute of Technology
AND
A. BOKSENBERG
Department of Physics and Astronomy, University College London
Received 1981 March 9; accepted 1981 July 10

ABSTRACT

High-resolution (0.8 Å FWHM) spectroscopic observations over the wavelength range from 3260 Å to 4900 Å are presented for the QSOs Q0002+051 ($z_{em} = 1.899$), Q0421+019 ($z_{em} = 2.051$), and the gravitationally lensed QSO, Q1115+080 ($z_{em} = 1.725$). We find, respectively, 28, 53, and 21 absorption lines in these three objects, from which a total of 11 absorption line systems are identified. Two of the QSOs show galactic Ca II $\lambda\lambda$3934, 3969 absorption. Four absorption systems with $z_{abs} > z_{em}$ are seen in Q1115+080; the velocities range from -360 to -1130 km s^{-1} relative to the QSO. Line profile fits to the absorption spectra are used to determine column densities and velocity dispersions within the absorbing clouds. Highly ionized lines of C IV $\lambda\lambda$1548, 1550, N V $\lambda\lambda$1238, 1242, and Si IV $\lambda\lambda$1393, 1402 are seen in many of the absorption systems.

The many unidentified lines shortward of Lyα emission are used to form an expanded sample of single Lyα absorption lines. The new data provide good statistics for $z_{abs} < 2$ and reveal a number density per unit redshift $N(z) = N_0(1 + z)^{\gamma}$ with $\gamma = 1.81 \pm 0.48$. This suggests a modest amount of cosmological evolution in the sense that there are more Lyα absorption lines at higher redshifts. The properties of the equivalent width spectrum of Lyα lines and the flatness of their two-point correlation function are in accord with our previous study.

Subject headings: line identifications — quasars

I. INTRODUCTION

We continue our study of the absorption features in QSOs with the three objects Q0002+051 ($z_{em} = 1.899$), Q0421+019 ($z_{em} = 2.051$), and Q1115+080 ($z_{em} = 1.725$). The first of these is the Michigan-Tololo object UM 18 and has been studied at low resolution in Lewis, MacAlpine, and Weedman (1979). The second object, Q0421+019, appears as a Parkes source and also as the Ohio source OF 036. It has been studied at low resolution by Schmidt (1977). These two objects were chosen simply because they are bright and were conveniently located at the time of observation. Q1115+080 is a set of gravitationally lensed images. A discussion of the geometry of the images and a description of low-resolution spectra may be found in Young *et al.* (1981). This QSO was observed primarily to look for Mg II $\lambda\lambda$2796, 2803 absorption lines from the hypothetical, intervening galaxy which is supposed to act as the lens. Such lines were not found, but a number of interesting absorption systems appear in Q1115+080 and are discussed in this paper. The lensed nature of this QSO does not disqualify it from being part of our uniform data set on bright, high-redshift QSOs.

Previous papers in this series include observations of six QSOs at high redshift in Young *et al.* (1979, hereafter Paper I), Sargent *et al.* (1979, hereafter Paper II), and Sargent *et al.* (1980, hereafter Paper III). Our previous work was concerned with absorption lines due to Lyα and to heavy elements, primarily at observed wavelengths longward of 4000 Å. In this paper, we have chosen QSOs at a somewhat lower redshift ($z_{em} = 1.725$–2.051) in order to obtain data on absorption lines from 3260 Å to 4000 Å. We found earlier that the single Lyα lines show no sign of clustering, and we attributed these lines to intergalactic clouds (Paper III). Surprisingly, however, we found no evidence for evolution of the clouds in cosmic time. The new observations, in particular, allow us to investigate the evolution in redshift of the Lyα absorption lines by improving the line samples at redshifts below $z_{abs} = 2$. In this investigation, we include data on Q0119−046 which has several other interesting properties which we discuss in a later paper. We also investigate the complex splitting structure of C IV $\lambda\lambda$1548, 1550 in some of the absorption systems of the three QSOs presented here. The nature of absorption complexes with $z_{abs} > z_{em}$ seen in Q1115+080 and also in Q0119−046 present some puzzling features. We shall discuss these complexes in our later paper on Q0119−046.

II. OBSERVATIONS AND REDUCTIONS

a) *Las Campanas Data*

Spectra of one of the QSOs (Q0002+051) were obtained on the Las Campanas 100 inch (2.54 m) reflector

[1] We regret the untimely death of Peter Young on 1981 September 5.—ED.

during 1980 November. We used the Shectman/Yanik photon-counting Reticon detector to observe simultaneously object and sky through 2″ × 4″ apertures on the two sides of the diode array. The 3744 pixels in the wavelength direction covered 1540 Å with a spectral resolution of 2.2 Å when a 600 line mm^{-1} grating was used in second order to provide a dispersion of 56 Å mm^{-1}. A liquid cell $CuSO_4$ filter and a WG 360 filter were used to isolate grating orders, and an inert gas He-Ne-A lamp was used to calibrate the wavelength scale. The flux standard LDS 235B was observed in order to remove the instrumental response from the spectra. In order to ensure maximum efficiency in the ultraviolet, an analog computer was used to orient the long axis of the aperture parallel to the atmospheric dispersion of the images. Polynomial fits to the inert gas lamp lines left residuals $\sigma = 0.11$ Å, and the data were rebinned on a logarithmic wavelength scale with 72.41 km s^{-1} per pixel. This was achieved without loss of resolution using the sampling theorem formula described in Young *et al.* (1981). All wavelengths in this paper are vacuum, heliocentric values. Further details of the individual observations may be found in Table 1.

b) *Palomar Observations*

Most of the spectra were obtained at the Cassegrain focus of the 200 inch (5.08 m) Hale reflector. We used the new Double Spectrograph (DS) to which was attached the University College London Image Photon Counting System (IPCS). The DS will be described in detail elsewhere. Briefly, the incoming light beam is split by a dichroic mirror in the DS into blue ($\lambda < 5300$ Å) and red ($\lambda > 5300$ Å) wavelength images. In our preliminary run, we replaced the dichroic mirror with an aluminized mirror to feed all light into the blue half of the spectrograph. The beams impinge upon Cassegrain collimators to generate a 146 mm diameter beam. On the blue side of the spectrograph, we used a 1200 line mm^{-1} grating blazed at 7500 Å (in first order). This was viewed by a folded Schmidt camera of focal length 229 mm to which was attached the IPCS. On each side of the spectrograph, superefficient coatings optimize transmission for the blue and red spectral ranges. With a 1″ slit at the Cassegrain focus (2.″54 per mm) and a reduction ratio of 10.1:1, the projected slit was 39 μm on the detector. When the grating was used in second order (18 Å mm^{-1}), we obtained a projected slit of 0.7 Å. The 35 mm IPCS field covered 630 Å. Some observations were made in the first order of the grating, at 36 Å mm^{-1}. This covers 1260 Å with a projected slit of 1.4 Å. Minor collimation problems led to spectral resolution slightly worse than the projected slit width; namely, 1.7 Å and 0.8 Å in first and second orders respectively.

Polynomial fits to the He-Ne-A comparison lamp observations left wavelength residuals $\sigma = 0.12$ Å and $\sigma = 0.06$ Å for the first and second order data respectively. These data sets were rebinned to logarithmic wavelength scales with 51.85 km s^{-1} and 25.93 km s^{-1} per pixel respectively. The instrumental response was removed using the observations of the flux standards EG 11 and EG 54. Further details of the individual observations may be found in Table 1.

Q1115+080 is a set of gravitationally lensed images (see Young *et al.* 1981 for details of the geometry). The seeing was generally quite poor (2″) while we observed this object, and so separate spectra of the faint images were not obtained. Q1115+080A was centered on the slit, and the images Q1115+080B, C were permitted to encroach upon the slit as little as possible.

c) *The Emission Lines*

The positions of various emission lines in our three QSOs were obtained by measuring suitably scaled plots. The equivalent widths were found by planimetry of the same plots. The resulting values may be found in Table 2, where we give more accurate emission redshifts for the QSOs. Comments on the individual objects follow:

Q0002+051. The previous redshift, $z_{em} = 1.89$, was

TABLE 1

JOURNAL OF OBSERVATIONS

Date (1980)	UT Start	Time (s)	λ-Range (Å)	FWHM (Å)	Dispersion (Å mm^{-1})	Telescope
			Q0002+051			
Nov 9	00^h40^m	8000	3530–5070	2.2	56	C100
Dec 10	02 13	6000	3260–3859	0.8	18	P200
			Q0421+019			
Dec 3	06 22	4527	3260–3859	0.8	18	P200
Dec 9	04 04	8000	3801–4421	0.8	18	P200
Dec 9	06 56	10000	4300–4916	0.8	18	P200
			Q1115+080			
Dec 1	10 30	7336	3801–4421	0.8	18	P200
Dec 2	10 42	7208	4300–4916	0.8	18	P200
Dec 9	10 50	7200	3260–3859	0.8	18	P200
Dec 12	10 33	5800	4460–5780	1.7	36	P200

TABLE 2

EMISSION LINES

Ion	λ_{rest} (Å)	λ_{obs} (Å)	z_{em}	W_{obs} (Å)	W_{rest} (Å)
			Q0002+051		
H I	1215.7	3524 ± 2	1.899 ± 0.002	163 ± 5	56.2 ± 1.7
N V	1240.1	3603 ± 6	1.905 ± 0.005	13 ± 2	4.5 ± 0.7
O I	1304.4	3782 ± 3	1.899 ± 0.002	6 ± 1	2.1 ± 0.3
Si IV+O IV]	1401.6[a]	4055 ± 4	1.893 ± 0.003	19 ± 1	6.5 ± 0.3
C IV	1549.1	4488 ± 2	1.897 ± 0.002	91 ± 4	31.4 ± 1.4
$\langle z_{em} \rangle$			1.899 ± 0.002		
			Q0421+019		
H I	1215.7	3708 ± 2	2.050 ± 0.002	121 ± 5	39.7 ± 1.6
N V	1240.1	3789 ± 6	2.055 ± 0.005	14 ± 2	4.6 ± 0.7
Si IV+O IV]	1401.6[a]	4269 ± 4	2.046 ± 0.003	15 ± 2	4.9 ± 0.7
C IV	1549.1	4724 ± 2	2.050 ± 0.001	41 ± 3	13.4 ± 1.0
$\langle z_{em} \rangle$			2.051 ± 0.002		
			Q1115+080		
H I	1215.7	3315 ± 6	1.727 ± 0.005	200 ± 30	73.5 ± 11.0
N V	1240.1	3384 ± 6	1.729 ± 0.005	17 ± 3	6.2 ± 1.0
Si IV+O IV]	1401.6[a]	3818 ± 4	1.724 ± 0.003	19 ± 2	7.0 ± 0.7
C IV	1549.1	4224 ± 3	1.727 ± 0.002	83 ± 4	30.4 ± 1.5
C III]	1908.7	5200 ± 4	1.724 ± 0.002	28 ± 3	10.3 ± 1.1
$\langle z_{em} \rangle$			1.725[b] ± 0.002		

[a] Assumes 85% O IV] λ1402.5 and 15% Si IV λ1396.8 as in Wills and Netzer 1979.
[b] PFUEI data gave $z_{em} = 1.7225 \pm 0.0005$ in Young *et al.* 1981.

determined from Lyα and C IV by Lewis, MacAlpine, and Weedman (1979). Our new redshift is slightly higher than this. However, the emission lines are markedly asymmetric with a more extended blue wing. We concluded that the line peak would provide a more accurate measure of the redshift of the underlying structure in which the QSO is embedded. This would be appropriate if the emission lines contained a significant flux from the "forbidden line region," which would contribute most to the peak. If not, the lesson of Seyfert galaxies is that the redshifts of permitted and forbidden line gas can differ by up to 3000 km s^{-1}. We also note that an asymmetric blue wing on the emission lines is a general property of high-redshift QSOs; we shall discuss this in a forthcoming paper where a large sample of objects is presented. Such a measurement involved the mean position of the points at which the lines were > 80% of their height above the continuum and was possible only for Lyα and C IV (the other lines had their "center of flux" measured). Particular weight should be given to the Lyα and C IV lines in Table 2 in estimating the redshift for this QSO.

Q0421+019. Schmidt (1977) measured $z_{em} = 2.048$. Our value, based on the "center of flux" of the symmetric lines gives a value in close agreement with this.

Q1115+080. This quintuply-imaged gravitational lens QSO was measured to be at $z_{em} = 1.7309$ by Weymann *et al.* (1980). Spectra of extraordinarily high signal-to-noise ratio were described in Young *et al.* (1981); $z_{em} = 1.7225 \pm 0.0005$ was determined from the C III] λ1909 emission line alone. That line may be perturbed slightly to the blue by emission of Al III λ1858. In measuring the new data, we used spline functions to interpolate across the strong absorption systems and measured the values shown in Table 2. The measurements on Lyα are uncertain because it was quite close to the blue edge of the spectrum and there was no continuum segment observed to the blue of the line. The C IV and C III] lines were satisfactory and give $z_{em} = 1.725 \pm 0.002$, in good agreement with the result in Young *et al.* (1981). The equivalent width of C III (83 Å) is in agreement with that found by Weymann *et al.* The C III] equivalent width was found to be only 28 Å, whereas 65 Å was found in Young *et al.* (1981) and Weymann *et al.* This seems to be most curious; we cannot obtain absolute fluxes and, consequently, we do not know which component of the spectrum varied. The weakness of C III] emission is seen clearly in Figure 5.

d) The Absorption Lines

In Paper I, we described methods of locating and measuring absorption line positions and strengths in QSO spectra. These methods were used to analyze the three new QSOs presented here, with one modification. Line positions were also determined by the centroid algorithm developed for use on binary star emission line data as described in Schneider and Young (1980). This gives superior results for weak lines and was used whenever the line was under 10 σ in strength. For stronger lines, we used the method described in Paper I. Checks of all lines using both methods found the same positions, to

TABLE 3

Q0002+051 ABSORPTION LINE LIST

No.	λ_{obs}	$\sigma(\lambda)$	W_{obs}	$\sigma(W)$	S/N	ID	z_{abs}	S1	S2
1	3307.84	0.16	0.80	0.13	7.1				
2	3315.34	0.10	3.06	0.16	7.6			*	
3	3332.18	0.09	0.32	0.07	8.5				
4	3336.76	0.10	2.91	0.15	8.4	HI(1215)	1.7448	*	
5	3344.73	0.09	0.60	0.08	8.8				
6	3354.95	0.08	0.66	0.07	9.9				
7	3369.02	0.11	0.39	0.07	10.7				
8	3377.70	0.08	2.27	0.09	11.2			*	*
9	3385.87	0.08	0.78	0.07	11.2				*
10	3396.78	0.10	0.78	0.08	11.4				*
11	3405.22	0.07	3.16	0.10	11.0			*	*
12	3414.02	0.09	0.85	0.07	12.0				*
13	3415.90	0.08	0.57	0.06	12.0				*
14	3425.42	0.08	2.69	0.10	12.7			*	*
15	3432.29	0.11	0.85	0.08	13.1				*
16	3447.14	0.09	0.20	0.04	14.4				
17	3453.59	0.09	0.27	0.04	16.0				
18	3456.27	0.09	0.43	0.05	15.6				
19	3469.65	0.12	0.32	0.05	17.8				
20	3472.55	0.07	0.77	0.04	18.4				*
21	3479.46	0.08	0.31	0.04	18.9				
22	3484.92	0.11	0.28	0.04	19.0				
23	3501.08	0.08	0.39	0.04	20.7				
24	3506.42	0.07	0.97	0.04	22.8			*	*
25	3514.86	0.09	0.30	0.03	28.8				
26	4248.72	0.22	0.79	0.11	20.3	CIV(1548)	1.7443		
27	4255.49	0.34	0.65	0.12	20.7	CIV(1550)	1.7441		
28	4411.34	0.25	0.76	0.12	20.0				

NOTE.—Region observed 3300–5070 Å. All wavelengths vacuum, heliocentric values. Starred lines are H I (λ1215) samples.

within the standard errors, for all but the weakest lines, where the centroid method is preferable (as is demonstrated by tests on simulated data).

The line lists are given in Tables 3–5, and the individual spectra, with absorption lines indicated, are shown in Figures 1–3. A line was required to be 5 σ in strength for acceptance into the lists. One-sigma errors are given in the line lists for positions and equivalent widths. The wavelength errors were computed from

$$\sigma^2(\lambda) = \sigma_*{}^2(\lambda) + \sigma_\lambda{}^2 , \quad (1)$$

where $\sigma_*(\lambda)$ is the standard deviation from counting statistics and σ_λ is the residual in the polynomial fit to the inert gas He-Ne-A frames (to allow for systematic distortions in the wavelength scale of magnitude σ_λ). The equivalent width W is also given with its one standard deviation error $\sigma(W)$. The S/N entry in Tables 3–5 gives the continuum signal-to-noise ratio as the continuum at that point divided by the 1 σ error for that point. The noise is equivalent to collecting $(S/N)^2$ counts in a Poisson process.

Note that we used a 5 σ strength limit to accept lines in this new work, whereas a 4 σ limit was used in Papers I and II. As explained in Paper I, however, the appearance of nonstatistical, upward fluctuations forced the limit to be 5 σ in most of the data in Papers I and II. Accordingly, to improve homogeneity, we decided to adopt a 5 σ limit everywhere in this and all subsequent work.

Both position and equivalent-width errors are based on counting statistics (with position errors as modified in eq. [1]). Systematic errors can be larger and will arise when the following conditions occur:

1. Subjective decomposition of obviously blended lines has been performed. Such cases can easily be seen in the figures.

2. The continuum is difficult to determine, especially in the vicinity of strong emission lines.

3. The line is broad and weak. Centroiding and strength measurements require subjective judgment as to the line width. In noisy data, this can be quite difficult.

The line lists are not complete to the 5 σ admission limit. Some portions of the spectra contained upward fluctuations of this order. These were not always at the positions of night-sky lines or at He I λ3889 where the comparison lamp was overexposed, producing a residual signal. We made our criteria more stringent when these abnormal, upward fluctuations appeared. This was demonstrated when we conducted an *a posteriori* line search at specific wavelengths for galactic Ca II absorption. Three 5–6 σ lines appeared as listed in Table 6. They are not included in our official *a priori* line lists since these lists were prepared prior to any redshift system analysis and must, subsequently, be adhered to strictly. Other absorption lines listed in Table 6 include additional identifications in already discovered absorption systems (see § III).

TABLE 4

Q0421+019 ABSORPTION LINE LIST

No.	λ_{obs}	$\sigma(\lambda)$	W_{obs}	$\sigma(W)$	S/N	ID	z_{abs}	S1	S2
1	3305.77	0.08	0.57	0.08	8.0				
2	3324.60	0.09	0.44	0.08	8.5	SiII(1260)	1.6377		
3	3334.13	0.12	1.17	0.12	9.0			*	
4	3338.57	0.10	0.34	0.07	9.2				
5	3351.69	0.10	1.02	0.10	9.2			*	
6	3353.76	0.10	0.35	0.07	9.3				
7	3363.76	0.09	0.54	0.07	9.8				
8	3366.23	0.08	0.37	0.06	9.8				
9	3372.89	0.11	0.92	0.09	10.4			*	*
10	3388.49	0.11	1.27	0.10	10.5			*	*
11	3401.48	0.12	1.11	0.10	11.1			*	*
12	3405.35	0.13	0.57	0.08	11.8				*
13	3413.18	0.10	0.59	0.07	11.9				*
14	3430.67	0.11	0.67	0.08	11.8				*
15	3449.65	0.12	0.60	0.08	11.6				*
16	3482.84	0.08	0.80	0.06	12.5				*
17	3501.87	0.08	1.19	0.07	12.4			*	*
18	3510.58	0.07	0.58	0.05	13.7				*
19	3519.43	0.10	0.84	0.07	13.0	CII(1334)	1.6372		
20	3523.72	0.09	0.55	0.06	13.7				*
21	3530.63	0.16	0.55	0.07	14.1				*
22	3534.82	0.12	0.54	0.07	14.5				*
23	3541.30	0.10	1.28	0.08	15.3			*	*
24	3558.70	0.09	0.29	0.05	14.7				
25	3589.65	0.10	0.36	0.05	15.2				
26	3597.36	0.08	0.68	0.06	15.5				*
27	3621.51	0.10	0.20	0.04	14.2				
28	3642.39	0.11	0.31	0.05	15.1				
29	3645.82	0.10	0.57	0.06	15.8	HI(1215)	1.9990		*
30	3651.70	0.16	0.46	0.07	15.9				
31	3655.65	0.12	0.72	0.07	16.1				*
32	3665.01	0.10	0.18	0.04	16.1				
33	3669.47	0.07	0.72	0.05	15.8				*
34	3675.23	0.08	0.57	0.05	15.5	SiIV(1393)	1.6369		
35	3677.93	0.08	2.55	0.08	15.0	SiIV(1393)	1.6388		
36	3699.94	0.09	1.01	0.05	24.3	SiIV(1402)	1.6376		
37	3707.19	0.07	1.20	0.04	26.5			*	*
38	3715.48	0.10	0.50	0.04	24.6	NV(1238)	1.9992		
39	3727.36	0.18	0.36	0.06	17.9	NV(1242)	1.9992		
40	3801.56	0.09	0.38	0.05	14.1	CIV(1548)	1.4555		
41	3807.87	0.12	0.35	0.06	13.2	CIV(1550)	1.4555		
42	3929.23	0.09	0.33	0.05	15.5	CIV(1548)	1.5379		
43	3935.62	0.09	0.49	0.05	15.4	CIV(1550)	1.5378		
44	4021.82	0.10	0.46	0.05	17.7	CIV(1548)	1.5977		
45	4028.36	0.11	0.32	0.05	17.2	CIV(1550)	1.5977		
46	4082.36	0.07	1.37	0.06	14.8	CIV(1548)	1.6368		
47	4084.00	0.07	1.22	0.05	15.7	CIV(1548)	1.6379		
48	4085.51	0.08	0.39	0.05	15.3	CIV(1548)	1.6389		
49	4089.18	0.07	1.15	0.06	14.6	CIV(1550)	1.6369		
50	4090.74	0.07	1.17	0.06	14.8	CIV(1550)	1.6379		
51	4092.31	0.08	0.49	0.05	14.4	CIV(1550)	1.6389		
52	4644.07	0.22	0.56	0.08	18.0	CIV(1548)	1.9997		
53	4651.26	0.20	0.54	0.08	18.4	CIV(1550)	1.9993		

NOTE.—Region observed 3300–4916 Å. All wavelengths vacuum, heliocentric values. Starred lines are H I (λ1215) samples.

Some comments on the individual line lists follow:

Q0002+051. This object lacks 0.7 Å resolution spectra longward of 3859 Å. The C100 data at 2.2 Å resolution has a very good signal-to-noise ratio (see Fig. 1) and serves to demonstrate that there is only one C IV doublet of modest strength in the spectrum. In not having 0.7 Å resolution data, we lose a factor of 2 in the line equivalent-width limit. Redshift systems below the C100 data threshold do not, in general, yield any lines that would be strong enough to contaminate a Lyα absorption line sample.

No absorption lines were reported in the previous low-resolution studies of this object. Our data show a total of 28 lines as listed in Table 3. The signal-to-noise ratio of the data is poor in the region from 3260 Å to 3300 Å, and so we restricted the line list to the region longward of 3300 Å.

Q0421+019. Schmidt (1977) found a single absorption line at 3675 Å (air wavelength) which we confirm in Table 4, where the absorption line list is expanded to 53 lines. An additional Ca II λ3969 line was found in our *a posteriori* search (given in Table 6) and leads us to suspect

TABLE 5

Q1115+080 ABSORPTION LINE LIST

No.	λ_{obs}	$\sigma(\lambda)$	W_{obs}	$\sigma(W)$	S/N	ID	z_{abs}	S1	S2
1	3273.47	0.07	1.87	0.07	14.6			*	*
2	3281.75	0.14	0.22	0.05	14.9	HI(1215)	1.6995		
3	3294.16	0.08	0.67	0.05	17.0	SiIII(1206)	1.7303		
4	3310.51	0.07	1.28	0.05	21.7			*	*
5	3316.94	0.07	0.68	0.03	24.5	HI(1215)	1.7285		
6	3319.06	0.07	0.53	0.03	25.4	HI(1215)	1.7302		
7	3321.39	0.06	0.97	0.03	25.0	HI(1215)	1.7321		
8	3325.44	0.07	2.07	0.05	24.2	HI(1215)	1.7355		
9	3344.50	0.11	0.40	0.05	17.6	NV(1238)	1.6997		
10	3384.77	0.07	0.63	0.03	25.5	NV(1238)	1.7323		
11	3395.63	0.07	0.40	0.02	27.2	NV(1242)	1.7322		
12	3812.57	0.11	0.25	0.04	19.4	SiIV(1393)	1.7355		
13	3837.23	0.09	0.16	0.03	22.2	SiIV(1402)	1.7355		
14	4179.68	0.14	0.33	0.05	23.5	CIV(1548)	1.6997		
15	4186.60	0.15	0.30	0.04	24.7	CIV(1550)	1.6997		
16	4223.87	0.10	0.28	0.04	23.6	CIV(1548)	1.7282		
17	4227.30	0.11	0.26	0.04	23.5	CIV(1548)	1.7305		
18	4229.81	0.07	1.00	0.04	24.7	CIV(1548)	1.7321		
19	4234.69	0.08	0.71	0.04	24.5	CIV(1548)	1.7352		
20	4236.83	0.07	0.88	0.04	24.0	CIV(1550)	1.7321		
21	4241.69	0.08	0.38	0.04	22.4	CIV(1550)	1.7352		

NOTE.—Region observed 3260–5780 Å. All wavelengths vacuum, heliocentric values. Starred lines are H I (λ1215) samples.

the line at 3935.62 Å in Table 4 also has a contribution from Ca II λ3934. This will be discussed in § IV. The region longward of 3300 Å was used to generate the line list since the short segment $\lambda < 3300$ Å is of poor quality.

Q1115+080. Weymann *et al.* (1980) report five absorption lines as being visible in this QSO. Not a single one of these is to be found in Table 5, where we list our 21 lines. Two of the lines reported by Weymann *et al.* appear in our galactic Ca II list in Table 6, but they are very weak, and we find it remarkable that these should be detected and a plenitude of much stronger lines missed. The QSO seems completely bereft of absorption lines longward of C IV emission, as may be seen in Figure 3.

III. ABSORPTION LINE SYSTEMS

a) Identification Procedures

These followed closely the methods described in Paper I. One refinement in the Bahcall (1968) search matrix method, as applied in Paper I, is that the redshift bin size was set to

$$\Delta z = (2\delta/3\lambda_c)(1 + z) \quad (2)$$

rather than a constant. Here δ is the redshift search acceptance window (1 Å) and λ_c the central observed wavelength of the spectra. This gives a relation

$$1 + z = (1 + 2\delta/3\lambda_c)^n \quad (3)$$

between redshift z and bin number n in redshift space.

The search program described in Paper I was used to comb each line list four times according to the following procedure:

1. The main pass used all observed lines together with the "short list" of candidate identification lines given in Paper I. We added N V $\lambda\lambda$1238, 1242 to the short list. This pass is sensitive to lines longward of Lyα emission, which are weighted 4 times more heavily than those shortward. Generally, all redshift systems with two or more lines visible longward of Lyα emission are discovered by this procedure. Inspection of doublet ratios and line strengths within an ionic species are used to eliminate obviously bogus systems. The quality of the observations is such that a single C IV $\lambda\lambda$1548, 1550 or Mg II $\lambda\lambda$2796, 2803 doublet gives a signal very much higher than the chance coincidences, when it is longward of Lyα emission.

2. The lines identified with redshift systems found in the first pass are removed. The second pass of the program uses only unidentified lines, again correlated against the short list of laboratory lines. In this pass, the number of identifications required for a possible absorption system is decreased relative to that required in step one.

3. A third pass correlates unidentified lines below Lyα emission with the short list.

4. All observed lines are correlated against C IV and Mg II resonance doublets alone. These transitions are usually very strong in absorption spectra; the aim is to discover obvious, strong doublets among the large number of absorption lines shortward of Lyα emission.

Finally, each candidate redshift is correlated against the long list of ground-state transitions in Morton and Smith (1973). This is used to uncover additional identifications in established systems. To this list, we added some special transitions of interest, e.g., H_2 lines.

Most of this activity turns out to be unproductive when dealing with observations of the quality obtained in this

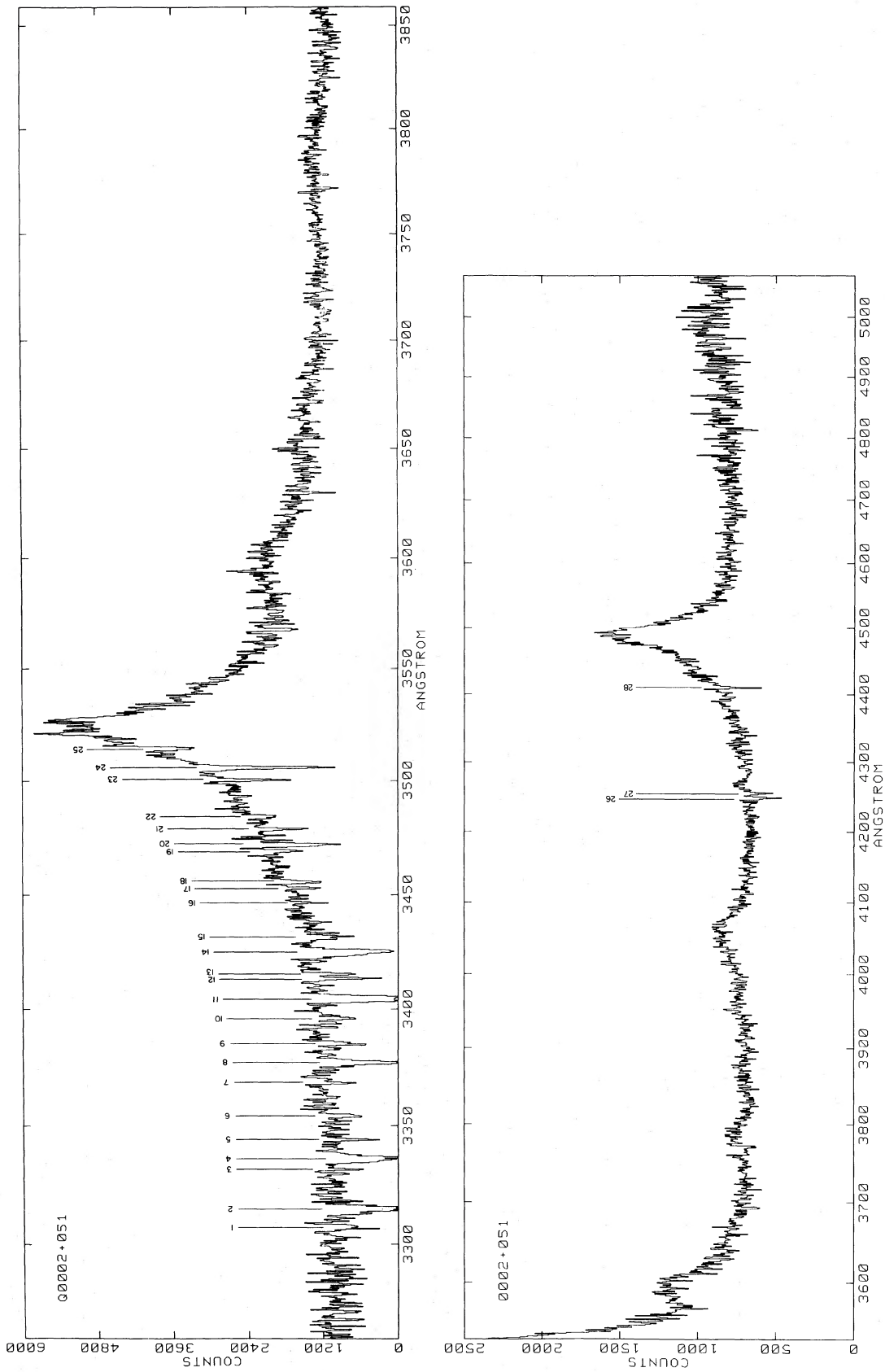

FIG. 1.—Spectra of Q0002+051. The first spectrum is P200 data at 0.8 Å resolution. Each bin is 25.9 km s^{-1}. The second spectrum is C100 data at 2.2 Å resolution where each bin is 72.4 km s^{-1}. The 28 absorption lines of Table 3 are marked. The spectra have been reduced to a linear flux scale of "counts" (which bear no relation to the count level in the original observations).

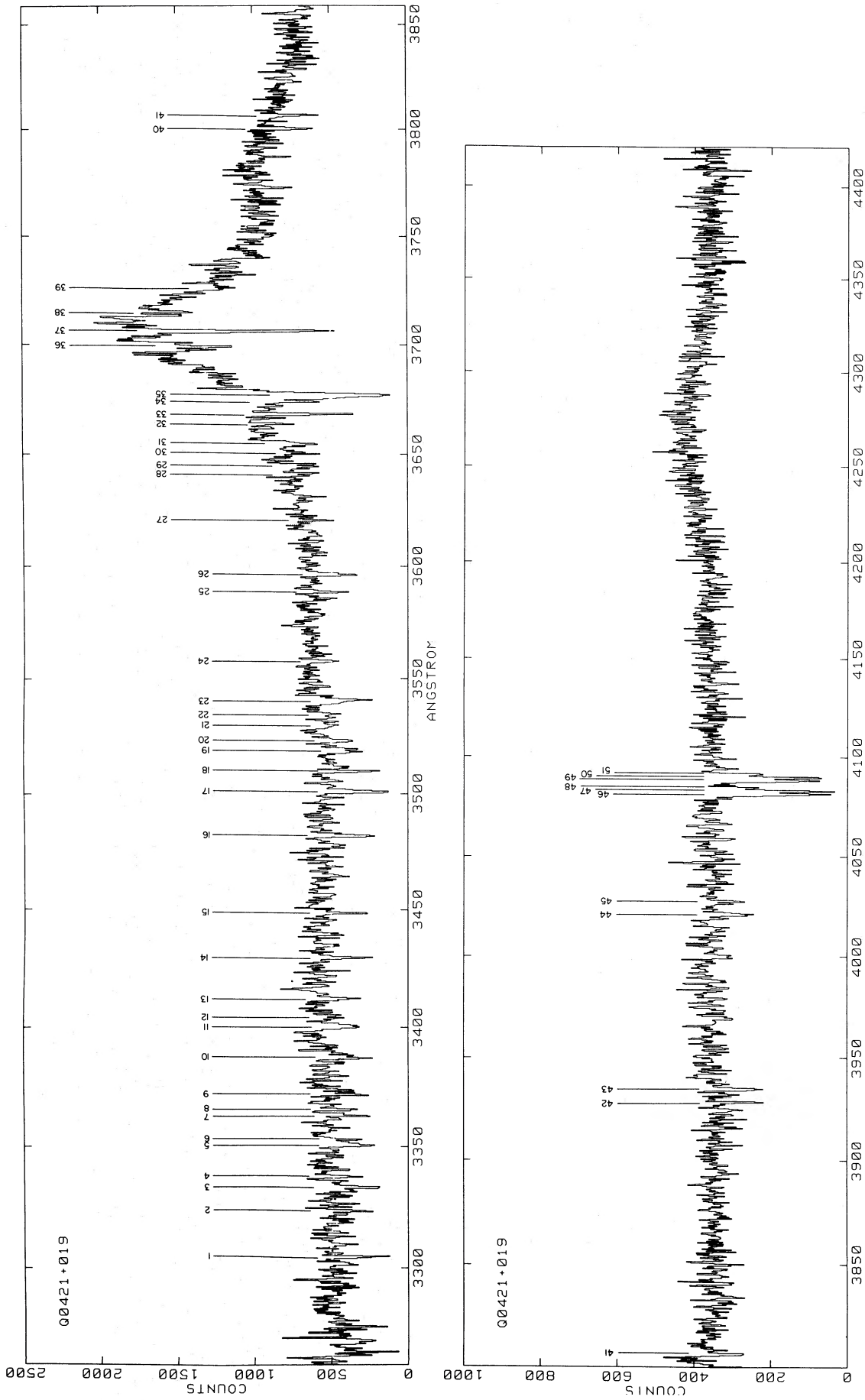

FIG. 2.—Spectra of Q0421+019. All spectra are P200 data at 0.8 Å resolution with 25.9 km s^{-1} in each bin. We have marked the 53 absorption lines given in Table 4. The spectra have been reduced to a linear flux scale. Slight rugosities at $\lambda\lambda$4047, 4359 are due to imperfect sky subtraction. A small, upward feature at λ3889 is due to overexposure of the photocathode by a He arc lamp.

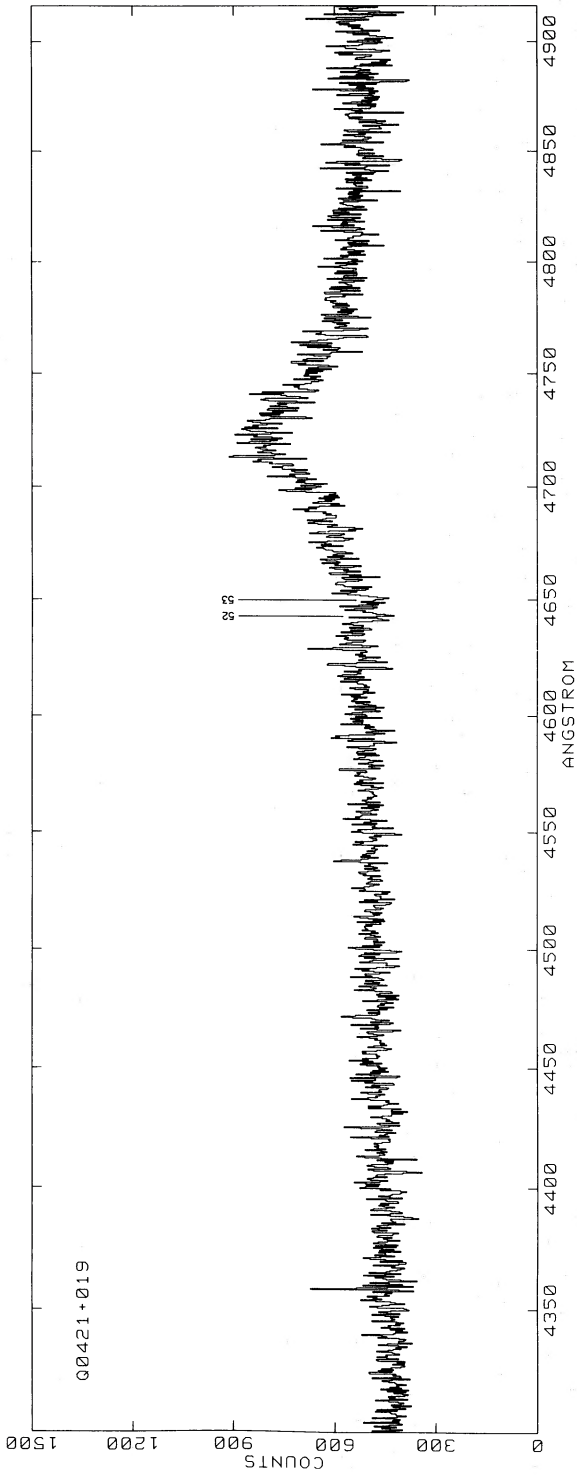

FIG. 2.—*Continued*

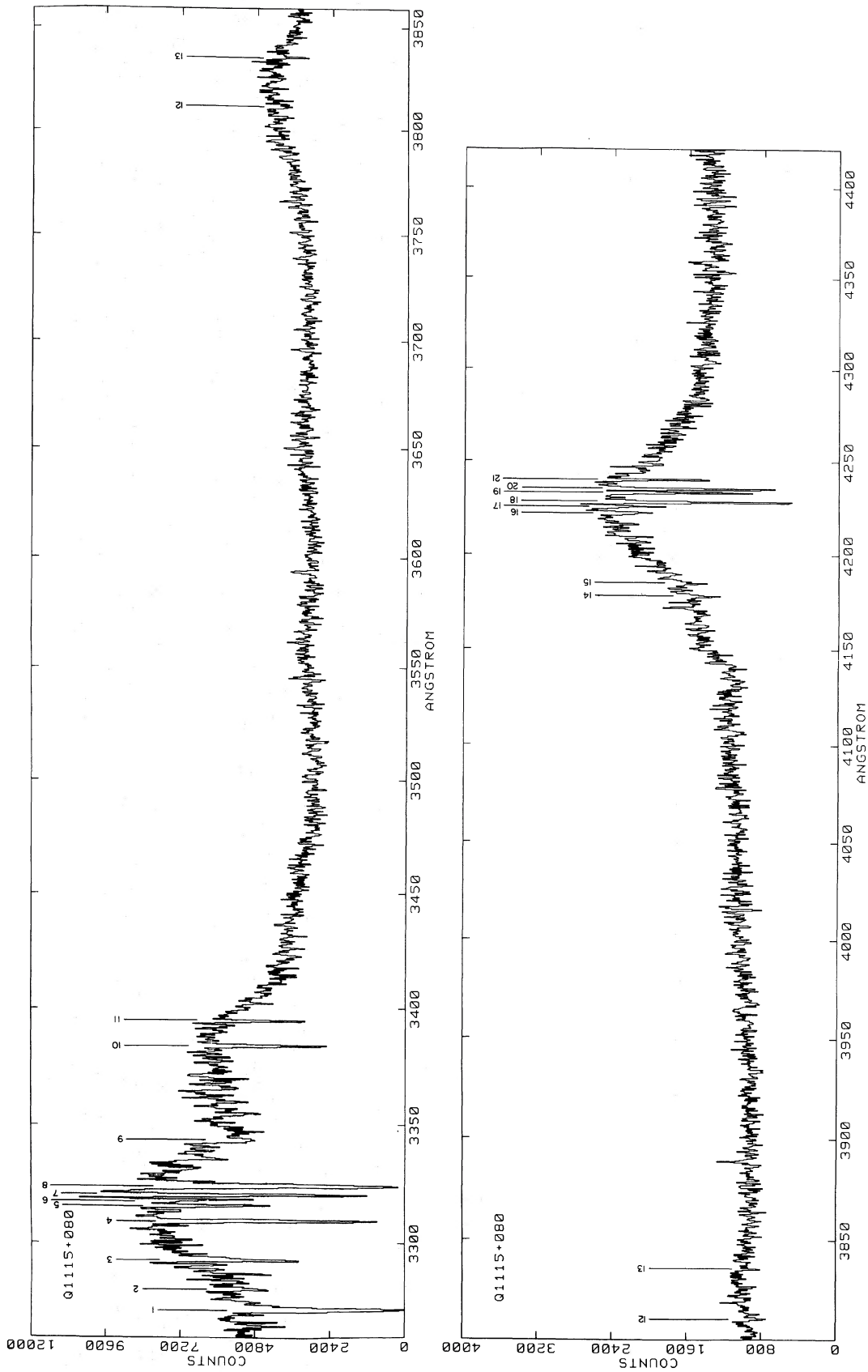

FIG. 3.—Spectra of Q1115+080. All spectra are P200 data. The three blue and ultraviolet spectra are at 0.8 Å resolution with 25.9 km s^{-1} per bin. The green spectrum has 1.7 Å resolution and has 51.8 km s^{-1} per bin. The 21 absorption lines in Table 5 have been marked. The spectra have been reduced to a linear flux scale. Rugosities near $\lambda\lambda 4359$, 5461, 5578 are due to imperfect sky subtraction, and at $\lambda 3889$ due to afterglow from the He arc lamp.

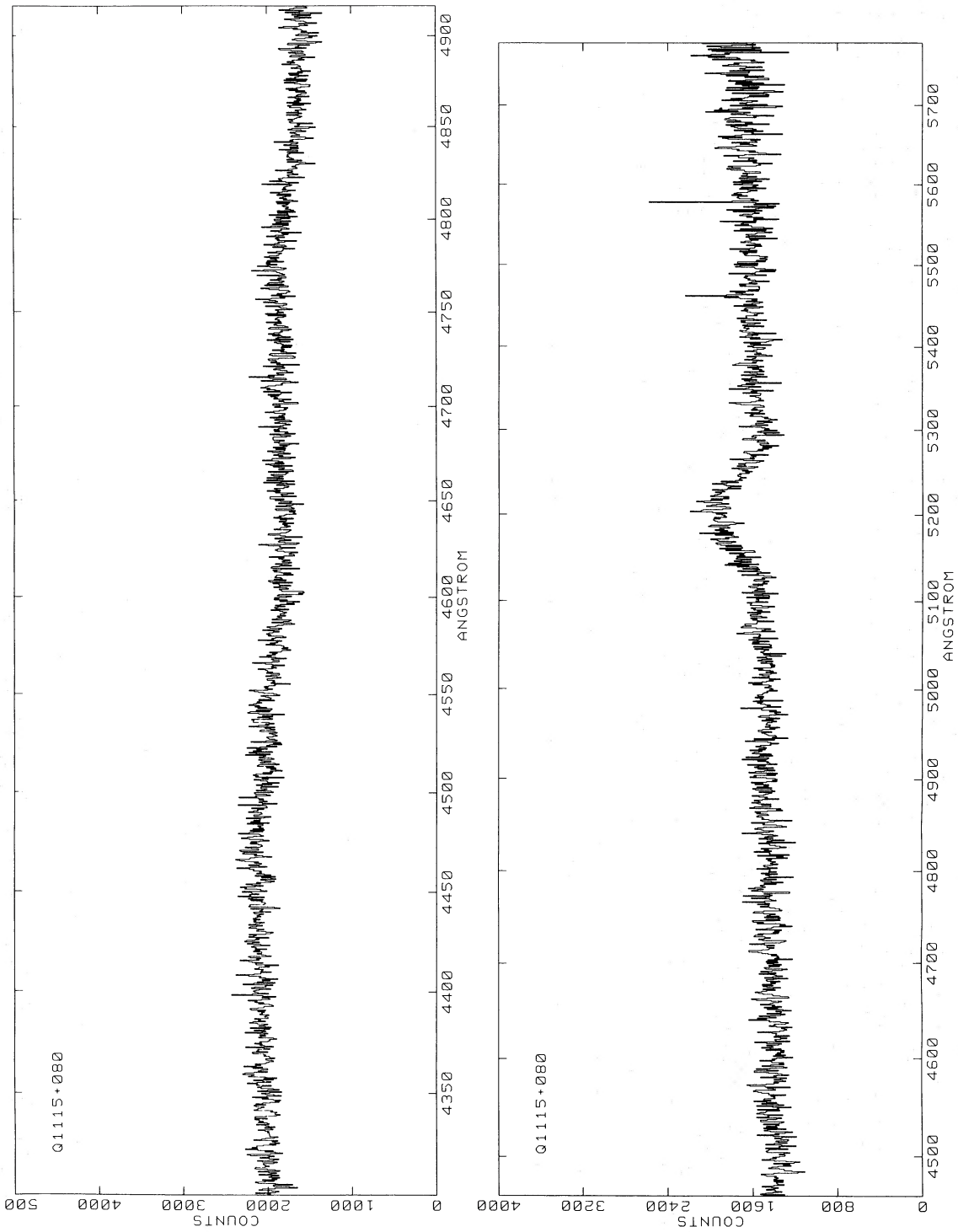

FIG. 3.—*Continued*

TABLE 6

ADDITIONAL ABSORPTION LINES[a]

λ	$\sigma(\lambda)$	W_{obs}	$\sigma(W_{obs})$	S/N	ID	z(ID)
			Q0421+019			
3267.11	0.10	0.97	0.11	7.5	N v (λ1238)	1.6373
3277.23	0.12	0.76	0.11	7.6	N v (λ1242)	1.6370
3970.30	0.11	0.27	0.04	19.8	Ca II (λ3969)	0.0002
			Q1115+080			
3355.72	0.08	0.22	0.03	20.5	N v (λ1242)	1.7001
3935.16	0.11	0.22	0.04	18.3	Ca II (λ3934)	0.0001
3969.45	0.13	0.22	0.04	20.2	Ca II (λ3969)	0.0000

[a] Lines found from an *a posteriori* quest for galactic Ca II absorption and additional lines in already discovered absorption systems. Wavelengths are vacuum, heliocentric values.

paper. The first pass of the program generally reveals all plausible redshift systems. These systems are usually obvious from a casual examination of suitable plots of the spectra and are secured when the wavelengths (which are accurate to better than 0.2 Å in these high-quality spectra) are checked.

After the above procedures, the spectra were reexamined in order to find marginally weak lines that might be in the well-established systems (e.g., missing members of doublets). This blatantly *a posteriori* search revealed a few extra lines which are listed in Table 6. These lines clearly should not be used in any future attempts to identify new redshift systems.

b) Q0002+051

The only absorption line system is listed in Table 7. Some comments on it follow:

$z_{abs} = 1.7444$. This system is firmly established by the isolated C IV $\lambda\lambda$1548, 1550 doublet longward of Lyα emission. The corresponding Lyα absorption has a slightly, but not unacceptably, discrepant wavelength. It may be mildly blended. No other lines appear in this redshift system.

One line longward of Lyα emission (number 28 in Table 3) remains unidentified. Only one line shortward of Lyα was identified. Most of the rest are presumably Lyα absorption lines, as we found in Paper I. The search for resonance doublets revealed only one possibility in identifying lines 21 and 22 in Table 3 as a C IV $\lambda\lambda$1548, 1550 doublet at $z_{abs} = 1.2474$. No additional lines could be found in this system which is thus not established. Only 3 out of 28 lines in the QSO are identified as being in "heavy element" absorption systems.

c) Q0421+019

Six absorption line systems of varying plausibility were found in this object. They are listed in Table 8, and some comments on the individual systems follow:

$z_{abs} = 0.0002$. An absorption line at λ3935 appears in Table 4 as part of the original line list. After this list was prepared, a special search for Ca II $\lambda\lambda$3934, 3969 absorption lines due to the Galaxy revealed a weak feature at λ3970. This pair of lines corresponds to the Ca II splitting to within 0.14 Å, and so we believe that galactic Ca II absorption is very likely present. See, however, our comments on $z_{abs} = 1.5378$ below.

$z_{abs} = 1.4555$. This is an isolated C IV $\lambda\lambda$1548, 1550 doublet. The line ratio is correct and the wavelength splitting precisely as expected. As discussed in Paper I, isolated C IV doublets longward of Lyα emission have a very small probability of being bogus in data of the quality being considered here.

$z_{abs} = 1.5378$. This, again, is an isolated C IV doublet. However, the long-wavelength member is stronger than the short-wavelength member because it coincides with the supposed Ca II λ3934 line in $z_{abs} = 0.0002$. While isolated C IV doublets generally give secure redshift systems, this unfortunate "locking" makes $z_{abs} = 1.5378$ only a possible system. No other lines were found (the expected other strong transitions being below our observed limit), and the λ3929 line did not fit in any other redshift system in Q0421+019. The Ca II λ3969 absorption should have its companion at 3935.41 Å, and the C IV λ1550 line should be at 3935.75 Å. The observed line is at 3935.62 Å and probably has about half its strength from each transition. The chance "line locking" is accurate to 0.34 Å, or 26 km s^{-1}.

$z_{abs} = 1.5977$. This is a quite secure redshift system consisting of an isolated C IV doublet with the correct line ratio and a wavelength splitting accurate to 0.14 Å.

$z_{abs} = 1.6375$. This is the only strong system in Q0421+019. The C IV $\lambda\lambda$1548, 1550 doublet has a clear triple structure (see Fig. 4). While the other lines in the system have a poorer signal-to-noise ratio, they are wide and consistent with this structure. The Si IV λ1393 line is too strong and a little to the red of its expected

TABLE 7

Q0002+051 ABSORPTION SYSTEM

No.	Ion	λ_{rest}	λ_{calc}	λ_{obs}	O-C	z_{abs}	W_{obs}	W_{rest}	Comments
1	H I	1215.67	3336.28	3336.76	+0.48	1.7448	2.91	1.06	Possibly blended.
	C IV	1550.77	4255.93	4255.49	-0.44	1.7441	0.65	0.24	
	C IV	1548.20	4248.88	4248.72	-0.16	1.7443	0.79	0.29	
					<z> =	1.7444			

TABLE 8

Q0421+019 ABSORPTION SYSTEMS

No.	Ion	λ_{rest}	λ_{calc}	λ_{obs}	O-C	z_{abs}	W_{obs}	W_{rest}	Comments
	Galactic Absorption.								
1	Ca II	3969.59	3970.38	3970.30	-0.08	0.0002	0.27	0.27	
	Ca II	3934.78	3935.57	3935.62	+0.05	0.0002	0.49	0.49	CIV(1550) in z=1.5378.
					<z> =	0.0002			
2	C IV	1550.77	3807.92	3807.87	-0.05	1.4555	0.35	0.14	
	C IV	1548.20	3801.61	3801.56	-0.05	1.4555	0.38	0.15	
					<z> =	1.4555			
3	C IV	1550.77	3935.54	3935.62	+0.08	1.5378	0.49	0.19	CaII(3934) in z=0.0002.
	C IV	1548.20	3929.02	3929.23	+0.21	1.5379	0.33	0.13	
					<z> =	1.5378			
4	C IV	1550.77	4028.44	4028.36	-0.08	1.5977	0.32	0.12	
	C IV	1548.20	4021.76	4021.82	+0.06	1.5977	0.46	0.18	
					<z> =	1.5977			
	Multiple system at z = 1.6368, 1.6379, 1.6389. Summed lines given with mean positions.								
5	C II	1334.53	3519.82	3519.43	-0.39	1.6372	0.84	0.32	
	C IV	1550.77	4090.16	4090.38	+0.22	1.6376	2.81	1.07	Triple structure clearly
	C IV	1548.20	4083.38	4083.44	+0.06	1.6375	2.98	1.13	visible in C IV doublet.
	N V	1242.80	3277.89	3277.23	-0.66	1.6370	0.76	0.29	
	N V	1238.82	3267.38	3267.11	-0.27	1.6373	0.97	0.37	
	Si II	1260.42	3324.36	3324.60	+0.24	1.6377	0.44	0.17	
	Si IV	1402.77	3699.81	3699.94	+0.13	1.6376	1.01	0.38	
	Si IV	1393.76	3676.04	3677.44	+1.40	1.6385	3.12	1.18	Probably blended.
					<z> =	1.6375			
6	H I	1215.67	3646.16	3645.82	-0.34	1.9990	0.57	0.19	
	C IV	1550.77	4651.22	4651.26	+0.04	1.9993	0.54	0.18	
	C IV	1548.20	4643.52	4644.07	+0.55	1.9997	0.56	0.19	
					<z> =	1.9993			

wavelength. Since it lies below Lyα emission, it is probably blended with a Lyα absorption feature. The N V $\lambda\lambda$1238, 1242 doublet was discovered *a posteriori*. The spectra have a poor signal-to-noise ratio below λ3300, and so it was decided, *a priori*, to include only lines above this wavelength. The N V doublet appears below 3300 Å, and the lines are thus relegated to Table 6. The C II λ1334 and Si II λ1260 lines are weak; it is not likely that both are chance coincidences given the observed density of lines below Lyα emission.

$z_{abs} = 1.9993$. A rather wide, shallow C IV doublet is visible near C IV emission. It is associated with a weak Lyα absorption. The lines have 7 σ significance and are probably real, but we do not regard this system as being secure.

These six systems identify all lines in Tables 4 and 6 longward of Lyα emission. Shortward of Lyα emission, the success rate is less good; only 6 out of 37 lines are identified. This is typical of the situation in high-redshift QSOs, as described in Papers I and II, for example. Most of these unidentified lines are thought to be Lyα absorptions with no other lines visible. No obvious C IV or Mg II doublets were found shortward of Lyα emission.

d) Q1115+080

Six absorption systems were found in Q1115+080, varying from certain to possible in their reliability. We give line lists for each system in Table 9, and we make the following comments:

$z_{abs} = 0.0000$. The special search for Ca II $\lambda\lambda$3934, 3969 lines due to our own Galaxy turned up two lines as shown in Table 6. We regard the evidence for interstellar Ca II to be reasonably secure.

$z_{abs} = 1.6998$. An isolated C IV $\lambda\lambda$1548, 1550 doublet is

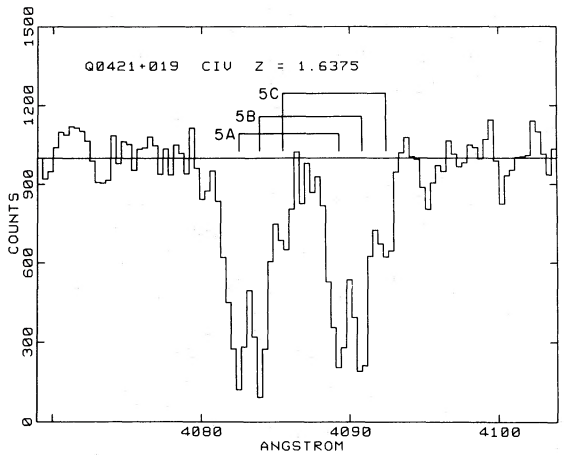

FIG. 4.—Detailed structure in the C IV $\lambda\lambda$1548, 1550 lines Q0421+019 at $z_{abs} = 1.6375$. Each bin is 25.9 km s^{-1} and the spectral resolution is 0.8 Å. The continuum has been divided out. The three principal components of the redshift system are indicated as 5A, 5B, and 5C.

seen in the blue wing of C IV emission. Further investigation revealed weak Lyα and N V $\lambda\lambda$1238, 1242 absorption at this redshift making the system secure. The N V λ1242 line was found *a posteriori* and is listed in Table 6.

$z_{abs} = 1.7283, 1.7304$. These two redshifts are part of an absorption complex just to the red of the peak of C IV emission. In both cases, the C IV λ1550 doublet member lies in the wing of a much stronger line in the complex. However, the absorption structure of the Lyα lines lends weight to our interpretation of the complex. Both these redshifts have a line in the expected position of Lyα. The system $z_{abs} = 1.7304$ may also have Si III λ1206, but since this falls shortward of Lyα emission it may be bogus. These two redshifts are not to be regarded as being secure, but it should be noted that the wavelength discrepancy from C IV λ1548 to Lyα is, in both cases, only 0.3 Å.

$z_{abs} = 1.7322, 1.7353$. C IV doublets in the complex at C IV emission, and a number of other lines, make these redshifts secure. There are strong Lyα absorption lines at both redshifts. There is a strong N V doublet in $z_{abs} = 1.7322$. A weak Si IV $\lambda\lambda$1393, 1402 doublet is probably present in the $z_{abs} = 1.7353$ redshift. In Figure 5, we show the absorption lines of C IV, N V, and Lyα in this absorption line complex.

All lines longward of Lyα emission in Q1115+080 are successfully identified. Two out of four lines are identified in the short segment of the spectrum below Lyα emission, to give an unusually high proportion of 19 identifications from 21 lines in total.

IV. ABSORPTION LINE COLUMN DENSITIES

a) *Profile Fitting and Curves of Growth*

Given a distribution function in velocity space $\psi(u)$ for a cloud of gas where

$$\int_{-\infty}^{\infty} \psi(u)du = 1 \qquad (4a)$$

and

$$u = v/v_s \qquad (4b)$$

with v being velocity and v_s some arbitrary scale in velocity space, we compute the line profile as follows. Let

$$H(a, u) = \frac{a}{\pi\psi(0)} \int_{-\infty}^{\infty} \frac{\psi(y)dy}{a^2 + (u - y)^2}, \qquad (5)$$

where a is the line-damping parameter in the relevant units,

$$a = \frac{\Gamma}{4\pi} v_s = \frac{\lambda_0 \Gamma}{4\pi} v_s, \qquad (6)$$

where v_s is the unit v_s in frequency space ($v_s/v_0 = v_s/c$), λ_0 is the rest wavelength of the line, v_0 its frequency, and Γ is the standard atomic reciprocal of the mean lifetime of the upper level (we are considering transitions from the ground state).

The quadrature in equation (5) is more conveniently expressed in the form

$$H(a, u) = \frac{1}{\pi\psi(0)} \int_{-\infty}^{\infty} \frac{\psi(u - a \sinh \chi)}{\cosh \chi} d\chi \qquad (7)$$

and, with $a = 0$, $H(0, u) = \psi(u)/\psi(0)$. The optical depth at any point in u-space is

$$\tau(u) = \tau_0 H(a, u), \qquad (8)$$

where τ_0 is the optical depth at $u = 0$ (supposing that $a = 0$),

$$\tau_0 = N_i W_f \psi(0)/\lambda_s, \qquad (9a)$$

$$W_f = (\pi e^2/m_e c^2) f \lambda_0^2 = 8.85 \times 10^{-13} f(\lambda_0/\text{cm})^2, \qquad (9b)$$

$$\lambda_s = (v_s/c)\lambda_0, \qquad (9c)$$

and N_i = ionic column density, f = oscillator strength of transition, and the other symbols have their usual meaning. The line profile is

$$s(u, \tau_0) = \exp[-\tau_0 H(a, u)], \qquad (10)$$

where $0 \leq s \leq 1$ is the residual flux at any point in the line, and the rest equivalent width is

$$\frac{W(\tau_0)}{\lambda_s} = \int_{-\infty}^{\infty} \{1 - \exp[-\tau_0 H(a, u)]\} du \qquad (11)$$

in wavelength units. For a Gaussian

$$\psi(u) = (2\pi)^{-1/2} \exp(-u^2/2), \qquad (12)$$

which has velocity dispersion $\sigma_v = v_s$ in velocity space, unity in dimensionless u-space, and $\sigma_\lambda = \lambda_s$ in wavelength space, the expression

$$\tau_0 = N_i W_f/\sigma_\lambda (2\pi)^{1/2} \qquad (13)$$

connects optical depth and column density in the usual way. A computer program was written to perform line profile and curve of growth calculations. The signal $s(u, \tau_0)$ was convolved with the spectrograph resolution function before comparison with the observations.

TABLE 9

Q1115+080 ABSORPTION SYSTEMS

No.	Ion	λ_{rest}	λ_{calc}	λ_{obs}	O-C	z_{abs}	W_{obs}	W_{rest}	Comments
	Galactic Absorption.								
1	Ca II	3969.59	3969.59	3969.45	-0.14	0.0000	0.22	0.22	
	Ca II	3934.78	3934.78	3935.16	+0.38	0.0001	0.22	0.22	
					<z> =	0.0000			
2	H I	1215.67	3282.07	3281.75	-0.32	1.6995	0.22	0.08	
	C IV	1550.77	4186.77	4186.60	-0.17	1.6997	0.30	0.11	
	C IV	1548.20	4179.83	4179.68	-0.15	1.6997	0.33	0.12	
	N V	1242.80	3355.31	3355.72	+0.41	1.7001	0.22	0.08	
	N V	1238.82	3344.57	3344.50	-0.07	1.6997	0.40	0.15	
					<z> =	1.6998			
3	H I	1215.67	3316.71	3316.94	+0.23	1.7285	0.68	0.25	
	C IV	1548.20	4223.95	4223.87	-0.08	1.7282	0.28	0.10	
					<z> =	1.7283			
4	H I	1215.67	3319.27	3319.06	-0.21	1.7302	0.53	0.19	
	C IV	1548.20	4227.21	4227.30	+0.09	1.7305	0.26	0.10	
	Si III	1206.51	3294.25	3294.16	-0.09	1.7303	0.67	0.25	Possibly bogus.
					<z> =	1.7304			
5	H I	1215.67	3321.45	3321.39	-0.06	1.7321	0.97	0.36	
	C IV	1550.77	4237.01	4236.83	-0.18	1.7321	0.88	0.32	
	C IV	1548.20	4229.99	4229.81	-0.18	1.7321	1.00	0.37	
	N V	1242.80	3395.58	3395.63	+0.05	1.7322	0.40	0.15	
	N V	1238.82	3384.70	3384.77	+0.07	1.7323	0.63	0.23	
					<z> =	1.7322			
6	H I	1215.67	3325.22	3325.44	+0.22	1.7355	2.07	0.76	
	C IV	1550.77	4241.82	4241.69	-0.13	1.7352	0.38	0.14	
	C IV	1548.20	4234.79	4234.69	-0.10	1.7352	0.71	0.26	
	Si IV	1402.77	3837.00	3837.23	+0.23	1.7355	0.16	0.06	
	Si IV	1393.76	3812.35	3812.57	+0.22	1.7355	0.25	0.09	
					<z> =	1.7353			

Only the strongest absorption lines have equivalent widths and profiles well enough determined for us to calculate column densities and Gaussian velocity dispersions. We discuss each such system in detail below.

b) Q1115+080: N v *in* $z_{abs} = 1.7322$

We first investigated the N v $\lambda\lambda$1238, 1242 doublet in the $z_{abs} = 1.7322$ system (see Fig. 5). A Gaussian velocity distribution

$$f(v) = (2\pi)^{-1/2} \exp(-v^2/2\sigma_v^2) \qquad (14)$$

was fitted to the N v doublet data. The best fit has

$$\sigma_v = 18.0 \pm 1.5 \text{ km s}^{-1},$$
$$\log \tau_0 = 0.14 \pm 0.08,$$
$$\log N_i = 14.38 \pm 0.08, \qquad (15)$$

for an "undamped" solution. This solution is shown in Figure 6. Since the doublet ratio is 1.45, a "damped" solution may be admissible. Computer simulations were run both with low-velocity dispersion profiles using the formalism of § IV*a* and with zero-velocity dispersion. As $\sigma_v \to 0$, the appropriate limits of the formulae in § IV*a* or direct computation gives a line profile optical depth

$$\tau(u) = \tau_c a^2/(a^2 + u^2) \qquad (16a)$$

with

$$\tau_c = \tau_0/\pi a \psi(0). \qquad (16b)$$

The central optical depth τ_c with no Doppler broadening does not equal τ_0 (the central optical depth as $a \to 0$, which diverges if there is no Doppler broadening while $\tau_0/\psi(0)$ remains finite). The ionic column density is

$$N_i = \pi a \tau_c \lambda_s / W_f \qquad (17a)$$

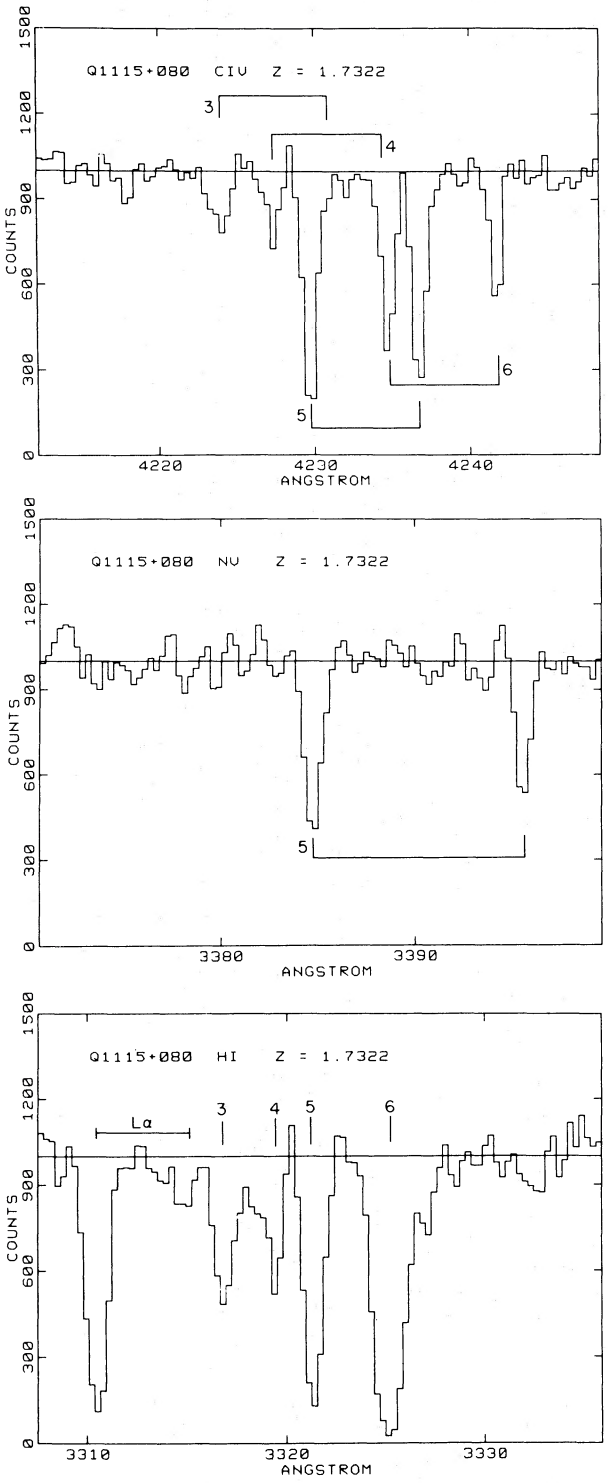

FIG. 5.—Detailed structure in C IV λλ1548, 1550; N V λλ1238, 1242, and Lyα absorption in Q1115+080 at $z_{abs} = 1.73$. The four redshift systems 3, 4, 5, and 6 are indicated. The N V lines appear only in system 5. The emission redshift $z_{em} = 1.725 \pm 0.002$ of the QSO is indicated in the Lyα plot by the horizontal error bar of length 2 σ. Thus most, or all, of the absorption redshifts shown are greater than the emission redshift. The continua in the spectra have been flattened out; their levels shown by the horizontal lines. Each bin is 25.9 km s^{-1} and the spectral resolution is 0.8 Å.

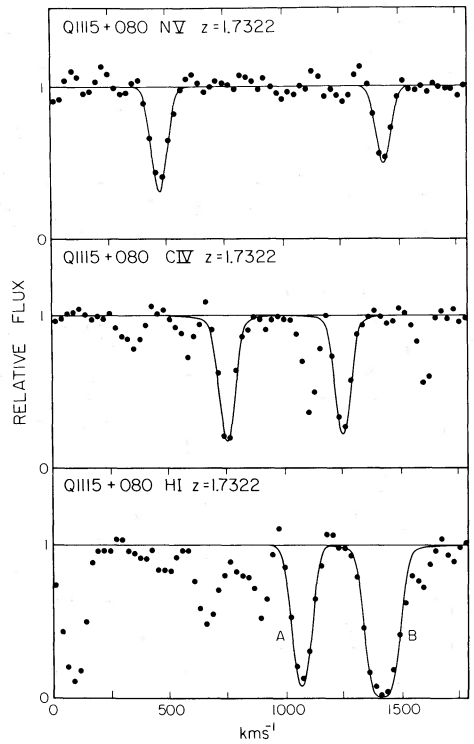

FIG. 6.—Profile fits to the absorption systems at $z_{abs} = 1.73$ in Q1115+080. The top graph shows the undamped solution fitted to N V λλ1238, 1242 in $z_{abs} = 1.7322$. The central graph shows the damped solution fitted to C IV λλ1548, 1550 in $z_{abs} = 1.7322$. The lowest graph shows the damped solution fitted to Lyα in $z_{abs} = 1.7322$ (marked A) and the solution for Lyα in $z_{abs} = 1.7353$ (marked B). Full details are given in § IV.

in our scaled units. In conventional units,

$$N_i = \tau_c(\Gamma/4c)(\lambda_0^2/W_f) = \tau_c(\Gamma/4c)(m_e c^2/\pi e^2 f) . \quad (17b)$$

The damped solution for the N V doublet ($\sigma_v = 0$) is

$$\log \tau_c = 7.18 \pm 0.04 ,$$
$$\log N_i = 17.77 \pm 0.04 . \quad (18)$$

When we consider systems with a small amount of Doppler broadening, we conclude

$$\sigma_v < 1.3 \text{ km s}^{-1} , \quad \log N_i = 17.77 \pm 0.04 , \quad (19)$$

describes the properties of the clouds. The thermal velocity dispersion is

$$\sigma_v = (kT/M)^{1/2}$$
$$= 2.4(T/10^4 \text{ K})^{1/2} \quad (\text{km s}^{-1}) \quad (20)$$

for the N V ion. The damped solution has the following problems:

1. It requires a low temperature $T < 3000$ K for the N V ions.

2. It implies an enormous total column density log $N_H > 21.8$ for cosmic abundances (and more if the metallicity is "sub-cosmic"). The weakness of Lyα absorption makes this rather unlikely as we shall see below.

Accordingly, we select the solution given by equation (15) as being more likely than that given by equation (19).

c) Q1115+080: C IV *Complex* $z_{abs} = 1.732$

As may be seen in Figure 5, this complex contains four C IV $\lambda\lambda$1548, 1550 doublets. Of those, two ($z_{abs} = 1.7322$, 1.7353) are relatively free of contamination by other lines and may be fitted independently. The other two are sufficiently blended that few deductions may be made about them.

The first doublet we shall consider is in the $z_{abs} = 1.7353$ system. The equivalent-width ratio is 1.87 ± 0.18, making this a virtually certain undamped solution. Upon fitting it with a Gaussian model, however, we encounter the difficulty that the λ1550 line is narrower than the λ1548 line. Further, a velocity dispersion that gives a doublet ratio of 1.87 yields much wider lines than are observed. This may be a clue that the velocity profile is not Gaussian. Since the line widths are of the order of the instrumental resolution, we cannot deconvolve the actual profile but must remain within the confines of the Gaussian model. Accordingly, we fitted the depths of the C IV lines and ignored the discrepancy in the red wing of the λ1550 line (this discrepancy may be statistical, anyway). The fitted doublet ratio is 1.65, and we find,

$$\sigma_v = 19 \pm 3 \text{ km s}^{-1},$$
$$\log \tau_0 = 0.00 \pm 0.07,$$
$$\log N_i = 14.09 \pm 0.06. \quad (21)$$

We now turn to the C IV doublet in the $z_{abs} = 1.7322$ system which has a ratio $R = 1.14 \pm 0.07$ and may, therefore, be either damped or undamped. It is near the logarithmic section of the curve of growth, and quantities are consequently difficult to measure with any precision. The minimum column density (thus maximum velocity dispersion) solution we found acceptable is

$$\sigma_v = 15 \text{ km s}^{-1},$$
$$\log \tau_0 = 0.81,$$
$$\log N_i = 14.80, \quad (22)$$

which has a doublet ratio of 1.15. It is, perhaps, slightly wider than the observed lines and seems definitely to be the lower limit. Solutions on the logarithmic part of the curve of growth were found satisfactory up to the maximum column density solution

$$\sigma_v = 7 \text{ km s}^{-1},$$
$$\log \tau_0 = 3.78,$$
$$\log N_i = 17.43, \quad (23)$$

which we show, for illustration, in Figure 6. The high column density solutions did not fit as well as the lowest one given in equation (22) because the doublet ratio decreased to 1.05. When this ratio began to rise again as the lines emerged on the square root part of the curve of growth, they developed damping wings which disagreed with the observations. For this reason, and also because of the N V doublet solution given in equation (15) for lines in the same redshift system, we prefer the low column density solutions for C IV with $\sigma_v \approx 15$ km s^{-1}. Considerable uncertainty remains in the column density, but $\log N_i \approx 15$.

The C IV lines in the $z_{abs} = 1.7283$, 1.7304 systems are too weak to provide reliable profile fits. Further, the C IV λ1550 line is blended with other members of the C IV complex in both cases.

d) Q1115+080: Lyα Complex $z_{abs} = 1.732$

The two Lyα lines at $z_{abs} = 1.7322$, 1.7353 are shown in Figure 5. The line at $z_{abs} = 1.7353$ is the stronger and shows hints of a damping wing profile. If we assume a Gaussian velocity distribution with $\sigma_v = 19$ km s^{-1}, then we may fit a profile (as shown in Fig. 6) to give the parameters

$$\log \tau_0 = 3.5 \pm 0.5, \qquad \log N_i = 17.0 \pm 0.5. \quad (24)$$

The uncertainties are large because the line is on the logarithmic part of the curve of growth, just beginning to emerge onto the square root part.

The Lyα line at $z_{abs} = 1.7322$ leads to greater uncertainty since the velocity dispersion of the gas in C IV is uncertain (even if the H I indeed has the same dispersion). If we take $\sigma_v = 15$ km s^{-1}, we find

$$\log \tau_0 = 1.8 \pm 0.3, \qquad \log N_i = 15.2 \pm 0.3. \quad (25)$$

Again, the latitude arises from the line being on the logarithmic part of the curve of growth. This fit is illustrated in Figure 6. If we take $\sigma_v = 7$ km s^{-1}, then we obtain

$$\log \tau_0 = 4.3 \pm 0.2, \qquad \log N_i = 17.4 \pm 0.2. \quad (26)$$

The fit is not quite so good as equation (25) because damping wings are starting to appear in the line. These are not supported by the data. The lower column density solutions are preferable, as we decided in § VI*c*, but the observations will support values from equations (25)–(26).

e) Q0421+019: C IV *Complex* $z_{abs} = 1.637$

This is an excellent example of the fine-scale velocity splittings that occur in strong absorption line systems. As illustrated in Figure 4, there are three components at our resolution of 0.8 Å. Inspection shows the doublet ratio to be about 1.1 with all three components having roughly this ratio. They are thus on the logarithmic part of the curve of growth, and we must suffer uncertainty in the column densities.

We first examined low column density solutions. The strongest pair of C IV lines was quite easy to fit with a pair of Gaussian clouds separated by 115 km s^{-1}. However, a residual signal in the blue wings of the lines could not be removed by increasing the velocity dispersion of the lower redshift cloud since this destroys the fit to the cores of the lines. The weak, highest redshift C IV doublet also presented a problem. The doublet ratio is nearly unity, and yet the line is both wide and shallow. No single cloud

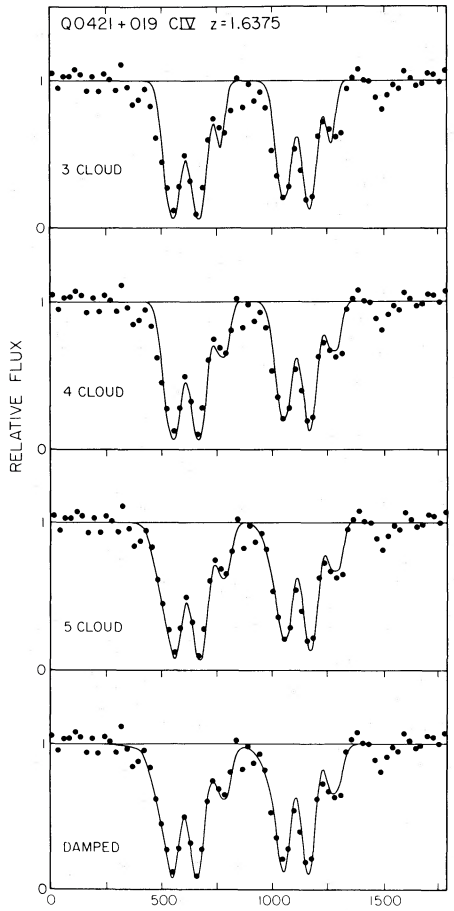

FIG. 7.—Profile fits to the absorption system at $z_{abs} = 1.6375$ in Q0421+019. The top graph shows an attempt to fit the three obvious components with an undamped, three-cloud model. Below, the fit is improved with four-cloud and five-cloud models. The lowest graph shows a damped, five-cloud model, with considerably greater column density, that also fits the data. Full details are given in § IV.

could provide a satisfactory fit; we show a typical attempt to fit it in Figure 7. If, instead, we employ two clouds close together, we can obtain the much more satisfactory fit also shown in Figure 7. Finally, a weak, additional cloud can remove the discrepancy in the blue wing of the C IV complexes. This five-cloud model is also shown in Figure 7 and has the following five components:

$$\begin{aligned}
&1: v = -180\,, \quad \sigma_v = 26\,, \quad \log \tau_0 = -0.60\,;\\
&2: v = -115\,, \quad \sigma_v = 23\,, \quad \log \tau_0 = \ \ 0.40\,;\\
&3: v = \ \ 0\,, \quad \sigma_v = 18\,, \quad \log \tau_0 = \ \ 0.70\,;\\
&4: v = +90\,, \quad \sigma_v = 3.2\,, \quad \log \tau_0 = \ \ 0.74\,;\\
&5: v = +128\,, \quad \sigma_v = 3.2\,, \quad \log \tau_0 = \ \ 0.74\,; \qquad (27)
\end{aligned}$$

which gives a total column density $\log N_i = 15.08$, of which a contribution $\log N_i = 14.98$ arises from the main pair of components 2 and 3. On the logarithmic part of the curve of growth, we may augment the column densities considerably by decreasing the Doppler broadening σ_v.

We have done this in a fourth model shown in Figure 7 where clouds 2 and 3 have had their velocities dropped to $\sigma_v = 6.4$ km s^{-1} and their optical depths raised to $\log \tau_0 = 4.0$ and 4.3 respectively. Minor adjustments were made to the other clouds to improve the fit. This gives a column density $\log N_i = 18.1$ which also fits the observations quite well. For much larger column densities, strong damping wings appear on the lines, and these are not observed.

V. LYMAN-ALPHA ONLY SYSTEMS

a) Samples

In Paper II, we obtained uniform samples of Lyα absorption lines in a number of high-redshift QSOs (denoted "sample 1") by: (1) taking all absorption lines below the emission redshift position of Lyα in the QSO; (2) eliminating all identified lines found not to be Lyα; and (3) eliminating all lines with a rest equivalent width $W < W_0 = 0.32$ Å, assuming each line to be a Lyα feature.

The data on the three QSOs in this paper and on Q0119−046 (which we discuss in a forthcoming paper) enhance the Lyα samples at the low-redshift end. We have selected all lines which obey conditions (1)–(3) above and marked them with an asterisk in Tables 3–5. The line list for Q0119−046 may be found in a later paper. A summary of the resulting samples is given in Table 10 for the four QSOs. It must be noted that in Paper III the decision was made to consider lines below Lyα emission in the QSO and reject all lines above Lyα emission. Thus, by the *a priori* dictates of Paper III, we must exclude the Lyα lines corresponding to the complexes of absorption with $z_{abs} > z_{em}$ that occur both in Q0119−046 and Q1115+080.

We also defined "sample 2" in Paper III with an equivalent-width cutoff $W_0 = 0.16$ Å. The wavelength range of "sample 2" for the four QSOs was defined by demanding that the signal-to-noise ratio in the spectrum be greater than 10. This ensures that lines with rest equivalent widths greater than 0.16 Å will not be lost in the continuum noise. The "sample 2" lines are also distinguished by asterisks in Tables 3–5. A summary of "sample 2" for our four QSOs is given in Table 10.

b) Mean Lyα Line Density

The total redshift coverage of "sample 1" in Table 10 is $\Delta z = 0.818$, and we find a total of 27 Lyα lines. The mean redshift of the sample is $\langle z \rangle = 1.83$. Thus, in the notation of Paper III, we find a mean density per unit redshift range ($\Delta z = 1$) of

$$N = 33.0 \pm 6.3 \qquad (28)$$

and densities normalized for cosmological effects:

$$N_0 = \begin{cases} N/(1+z) & = 11.7 \pm 2.2 \quad (q_0 = 0)\,, \\ N/(1+z)^{1/2} & = 19.6 \pm 3.7 \quad (q_0 = \tfrac{1}{2})\,. \end{cases} \qquad (29)$$

Since the mean values for the QSOs in Paper III were $N_0 = 17.6 \pm 1.3$ ($q_0 = 0$) and $N_0 = 32.8 \pm 2.4$ ($q_0 = \frac{1}{2}$)

TABLE 10

THE LYMAN-ALPHA SAMPLES

QSO	z_{em}	λ (Lyα) (Emission)	λ-Range	z_{abs}-Range	No. of Lyα Lines	N	W_0
			Sample 1				
Q0002+051	1.899	3524	3300–3524	1.715–1.899	6	32 ± 13	0.32
Q0119−046	1.937	3570	3260–3570	1.682–1.937	11	43 ± 13	0.32
Q0421+019	2.051	3709	3300–3709	1.715–2.051	8	24 ± 8	0.32
Q1115+080	1.725	3313	3260–3313	1.682–1.725	2	(47)	0.32
			Sample 2				
Q0002+051	1.899	3524	3360–3524	1.764–1.899	10	74 ± 23	0.16
Q0119−046	1.937	3570	3280–3570	1.698–1.937	16	67 ± 17	0.16
Q0421+019	2.051	3709	3370–3709	1.772–2.051	19	68 ± 16	0.16
Q1115+080	1.725	3313	3260–3312	1.682–1.725	2	(47)	0.16

for a sample with a mean redshift $\langle z \rangle = 2.44$, we see significant discrepancies between the densities in equation (29) and those in Paper III. The discrepancy is 3.0 σ for $q_0 = \frac{1}{2}$ and 2.3 σ for $q_0 = 0$ suggesting that, while $q_0 = 0$ is a better fit than $q_0 = \frac{1}{2}$, there is now evidence for evolution in the number of Lyα lines in the sense that there are more lines at higher redshifts.

It should also be noted that the mean Lyα densities observed in the four individual QSOs in "sample 1" as listed in Table 10 do not differ significantly from the value given in equation (28). The samples are small, and so the statistical power of the test is slight, but, for the first three objects in Table 10, we find a formal $\chi_2^2 = 1.86$ for deviations from the mean value given in equation (28). This is to be compared with the tabulated value $\chi_2^2(0.95) = 5.99$ and indicates that the QSOs have the same line density to within the statistical fluctuations within small samples. A slightly stronger statement may be made using "sample 2" as listed in Table 10 when the deviations have $\chi_2^2 = 0.08$. This is quite small [note that $\chi_2^2(0.05) = 0.103$] but shows that the first three QSOs in Table 10 have identical sample 2 line densities.

c) *Evolution in Lyα Absorption Line Density*

In order to illustrate the current data set on Lyα absorption mean densities, we have created four bins of Lyα lines as listed in Table 11. Bin 1 consists of the new data in this paper plus the data in Paper III for $z \leq 1.9$. Bins 2, 3, and 4 are the data in Table 10 of Paper III for $1.9 < z \leq 2.3$, $2.3 < z \leq 2.7$, and $z > 2.7$ respectively.

TABLE 11

LYMAN-ALPHA MEAN DENSITIES

Bin No.	$\langle z \rangle$	Δz	No. of Lines	N	N_0 ($q_0 = 0$)
1	1.80	1.02	39	38 ± 6	13.6 ± 2.1
2	2.12	0.90	54	60 ± 8	19.2 ± 2.6
3	2.55	1.10	69	63 ± 8	17.7 ± 2.3
4	2.95	0.50	38	76 ± 12	19.2 ± 3.0

These points are plotted in Figure 8 together with a line having the assumed functional form

$$N(z) = N_0(1 + z)^{\gamma}, \tag{30}$$

from which we find

$$\gamma = 1.81 \pm 0.48 \tag{31}$$

(1 σ error given). This is to be compared with the value of $\gamma = 0.48 \pm 0.54$ found in Paper III. Our augmented Lyα sample has improved the low-redshift statistics and yields fewer Lyα lines that in the limited data for $z < 2$ in Paper III. The mean Lyα line density of the new total sample which has $\langle z \rangle = 2.35$ is

$$N(2.35) = 57 \pm 4 \tag{32}$$

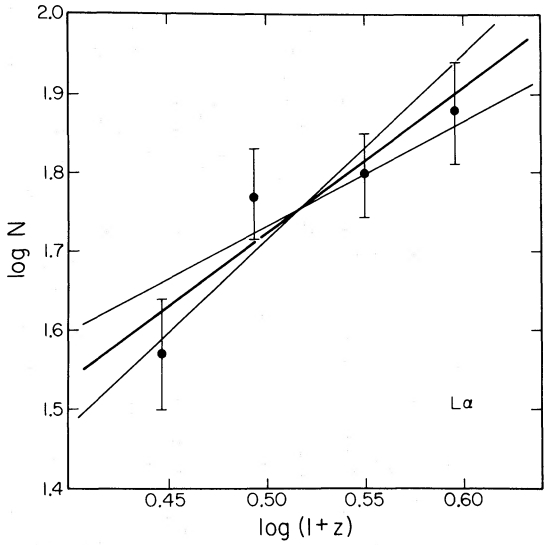

FIG. 8.—Lyα mean density per unit redshift N versus redshift z in logarithmic coordinates. Data from Paper III define the three right-hand points, and the new data in this paper plus some old data from Paper III define the left most point. The error bars are of length 2 σ. The best-fitting regression line $N = N_0(1 + z)^{\gamma}$ is shown with flanking 1 σ deviates; $\gamma = 1.81 \pm 0.48$.

and does not differ significantly from the value $N(2.44) = 61 \pm 4$ found in Paper III. An increased data sample at the high-redshift end would lead to improved values of γ.

Cosmological models with *unevolving cloud populations* predict a slope

$$\gamma = (1 + q_0 z - q_0)(1 + 2q_0 z)^{-1}, \quad (33)$$

which varies from $\gamma = 1$ ($q_0 = 0$) through $\gamma = \frac{1}{2}$ ($q_0 = \frac{1}{2}$) to $\gamma = (1 - \langle z \rangle^{-1})/2 = 0.29$ ($q_0 = \infty$). The value of γ found in equation (31) cannot yet rule out the absence of evolution for the Lyα clouds in a $q_0 = 0$ cosmology. On the other hand, it would indicate evolution at the 2 σ level or more for any value of $q_0 > 0.05$.

One is impressed by the apparently greater Lyα line densities in higher redshift QSOs (e.g., compare Figs. 1, 2 with the PKS 2126−158 observations in Paper I). However, since the observed equivalent width $W_{\rm obs} = W(1 + z)$, the line blanketing $B(z)$ will attract an extra factor $1 + z$. Since cosmological effects cause the observed number of lines per unit redshift to vary as

$$N(z) = N_0(1 + z)^{\gamma}, \quad (34)$$

then

$$B(z) = B_0(1 + z)^{\gamma + 1}, \quad (35)$$

and the blanketing increases with redshift with a power $\gamma + 1 = 2.81 \pm 0.48$. This is a factor of ~ 2.7 from redshift $z = 1.8$ to $z = 3.0$ and would explain the striking difference between the spectra.

d) Lyα *Line Equivalent-Width Spectrum*

In Paper III, we deduced a rest equivalent-width spectrum for the Lyα lines with the functional form

$$n(W) = (N_*/W_*) \exp(-W/W_*). \quad (36)$$

We have taken a sample 2 for the four QSOs and have fitted equation (36) using the technique of maximum likelihood estimation as described in Paper III. In this, we take a distribution function

$$f(W; W_*) = W_*^{-1} \exp[(W_0 - W)/W_*] \quad (37)$$

normalized to give

$$\int_{W_0}^{\infty} f(W) dW = 1 \quad (38)$$

and maximize, with respect to W_*, the quantity

$$\sum_{k=1}^{L} \ln f(W_k; W_*) = -L \ln W_* + \sum_{k=1}^{L} \frac{(W_0 - W_k)}{W_*} \quad (39)$$

for a sample of lines $W_k (1 \le k \le L)$. The standard deviation of the estimate of W_* is given by

$$\sigma(W_*) = W_* L^{-1/2} \quad (40)$$

(this may be computed from eq. [8] in Paper III). The result is

$$W_* = 0.232 \pm 0.034, \quad (41)$$

and the normalization of equation (36) is the number density of lines per unit redshift and is found to be

$$N_* = 135 \pm 20 \quad (42)$$

from the analysis of sample 2.

In Paper III, we found $W_* = 0.36$ and $N_* = 154$ from the line samples contained therein. These appear to differ significantly from the values given in equations (41) and (42). However, after corrections for line blending, we found $W_* = 0.25$ and $N_* = 250$ so that the slope of the corrected spectrum is identical to equation (41), at least to within the errors. The value of N_* is higher than equation (42) and simply reflects the higher line densities in the higher redshift data in Paper III. The blending corrections to the values given in equations (41) and (42) are negligible because of the higher signal-to-noise ratio in the new data and, more importantly, the lower line densities for $z < 2$ and thus allow us to compare these uncorrected values directly with the results in Paper III.

The size of sample 2 (47 lines) in the new data is too small for us to check whether the functional form of equation (36) is a valid description of the equivalent-width spectrum for $z < 2$ only. Such a check would clearly be desirable with an augmented data set.

e) Lyα *Correlation Function*

In Paper III, we computed the correlation function in redshift for the Lyα lines; we found it to be flat on all observed distance scales. In order to calculate the correlation function for the new data (with $z < 2$), we note that the comoving coordinate of a cloud at redshift z is

$$S_0(z) = 2[1 - (1 + z)^{-1/2}] \quad (43)$$

for a cosmological model with $q_0 = \frac{1}{2}$. (This model was used in Paper III, and so for direct comparison we shall continue to use $q_0 = \frac{1}{2}$.) The comoving separation between two clouds at redshifts z_1 and z_2 is given by

$$s_0 = S_0(z_2) - S_0(z_1), \quad (44)$$

where both S_0 and s_0 are measured in units of the Hubble radius, c/H_0. Sample 2 in Table 10 was used to compute the correlation function as prescribed in Paper III. We omitted Q1115+080 because of the small numbers of lines in the small wavelength range available. The results of the analysis of sample 2 for the other three QSOs are shown in Figure 9. The correlation function is flat on all scales $s_0 < 0.0222$ except for the deficit for $s_0 < 0.0005$ caused by line blending and the finite resolution (0.8 Å) of the observations. The relation between Hubble flow velocity difference for the pairs of clouds and the corresponding comoving coordinate splitting is

$$v = cs_0(1 + z)^{1/2}. \quad (45)$$

This expression gives the Hubble flow velocity difference corresponding to a splitting s_0 as seen by an observer in one cloud at the epoch when the observed radiation transversed the cloud.

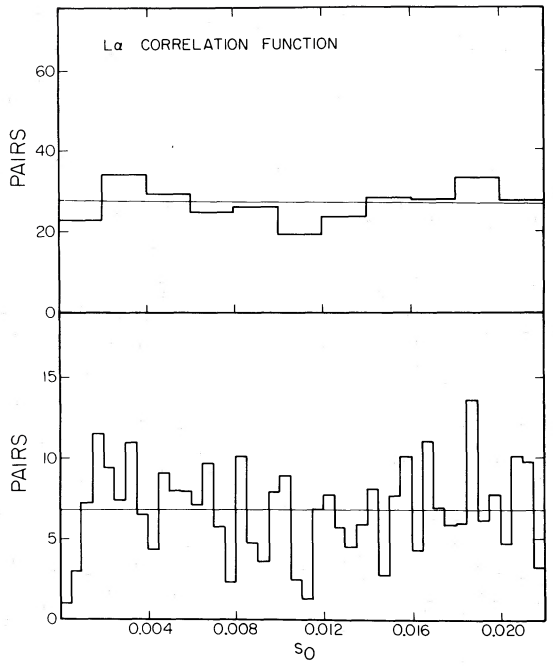

FIG. 9.—Correlation function for pairs of Lyα lines. The top graph has bins $\Delta s_0 = 0.002$ (s_0 = comoving coordinate separation in units of the Hubble radius c/H_0) and the lower graph is the same data binned with $\Delta s_0 = 0.0005$. Poissonian mean levels are indicated by horizontal lines. The bins correspond to relative Hubble flow velocities of 1000 and 250 km s^{-1} for the two graphs.

VI. DISCUSSION AND SUMMARY

a) The Metal-Line Absorption Systems

Observations of Q0002+051, Q0421+019, and Q1115+080 have shown the large number of absorption lines usually found in the spectra of high-redshift QSOs. Line lists containing 28, 53, and 21 lines, respectively, were prepared for the three QSOs. Using uniform search procedures, a total of 11 absorption systems were found in the three QSOs. All of these were distinguished by containing a C IV $\lambda\lambda$1548, 1550 doublet longward of Lyα emission in the QSO. Two of the QSOs showed Ca II $\lambda\lambda$3934, 3969 doublets due to galactic interstellar absorption.

The stronger lines were fitted with theoretical profiles in order to assess column densities and velocity structure. The system $z_{abs} = 1.637$ in Q0421+019 shows a clear triple structure in C IV $\lambda\lambda$1548, 1550. Components at $v = -115, 0$, and $+109$ km s^{-1} were best fitted with a five Gaussian cloud model, but the column density was indeterminate. The absorption system structure seems typical of the fine splittings generally seen at high spectral resolution.

A complex of four absorption systems with $z_{abs} > z_{em}$ was discovered in the gravitationally lensed object Q1115+080. The velocities are -360, -580, -790, and -1130 km s^{-1} relative to the QSO (whose emission redshift is uncertain by 220 km s^{-1}). The emission complex shows C IV doublets, Lyα lines, and in one system a N V $\lambda\lambda$1238, 1242 doublet. No low-ionization species (e.g., C II, Si II) are observed. Profile fits to the strongest two redshift systems yield velocity structure and column densities.

The object Q0119−046 also shows an absorption complex with $z_{abs} > z_{em}$ which seems similar to that in Q1115+080. We discuss our data for Q0119−046 in a later paper and defer our discussion of the origin and nature of these absorption complexes until then.

b) The Lyα Absorption Systems

The number density of absorption lines shortward of Lyα emission in the three QSOs presented here is, as usual, much higher than the density longward of Lyα emission. We prepared uniform samples of single Lyα absorption lines in these three objects and included in our analysis a similar sample from Q0119−046. From these data which improve the available Lyα samples for $z_{abs} < 2$, and from the data in Paper III, we conclude:

1. The number density versus redshift relation for the Lyα systems, if assumed to be of the form $N(z) = N_0(1+z)^{\gamma}$, gives a best-fit value of $\gamma = 1.81 \pm 0.48$. This suggests evolution in the cloud density in the sense that more clouds are visible at higher redshifts. Cosmological models with $q_0 = 0$ have $\gamma = 1$ if the clouds do not evolve, and such a model is still consistent with our data. Any model with $q_0 > 0.05$ and without evolution in the cloud density is inconsistent with our data at the statistical level of 2 σ or more.

2. The equivalent-width spectrum, if assumed to be of the form $n(W) = (N_*/W_*) \exp(-W/W_*)$ has maximum likelihood estimates $W_* = 0.232 \pm 0.034$ and

$$N_* = 135 \pm 20$$

from our data. After considering the effects of blending in the higher line density samples of Paper III, the equivalent-width spectrum parameter W_* found here is not statistically different from that in Paper III ($W_* = 0.25$).

3. The correlation function in the new sample of Lyα lines is flat on all scales from 250 to 11,000 km s^{-1}. This is in accord with our findings for the higher redshift Lyα lines discussed in Paper III.

The inferred evolution of Lyα lines, if real, may be achieved through a reduction in the number of clouds at lower redshift by reducing their size or reducing their optical depth by changes in the ionization balance with redshift. We are not yet in a position to discuss the physical evolution of the clouds any further than our speculations in Paper III. However, we note that the newly discovered tendency for the Lyα line density to decrease at lower redshifts is in harmony with the fact that no Lyα absorption lines have been found in ultraviolet spectra of 3C 273 (Ulrich *et al.* 1980).

We are indebted to J. B. Oke for finishing the construction of the Palomar Double Spectrograph in time for our observing run. We thank J. Fordham, K. Shortridge, and D. Walker for assistance with the IPCS. W. L. W. S. was

supported by grant AST 78-23795 from the National Science Foundation, and P. Y. was supported by grant AST 80-03398. The work of A. B. and the development of the IPCS detector which made these observations possible were supported by the U.K. Science Research Council.

REFERENCES

Bahcall, J. N. 1968, *Ap. J.*, **153**, 679.
Lewis, D. W., MacAlpine, G. M., and Weedman, D. W. 1979, *Ap. J.*, **233**, 787.
Morton, D. C., and Smith, W. H. 1973, *Ap. J. Suppl.*, **26**, 333.
Sargent, W. L. W., Young, P. J., Boksenberg, A., Carswell, R. F., and Whelan, J. A. J. 1979, *Ap. J.*, **230**, 49 (Paper II).
Sargent, W. L. W., Young, P. J., Boksenberg, A., and Tytler, D. 1980, *Ap. J. Suppl.*, **42**, 41 (Paper III).
Schmidt, M. 1977, *Ap. J.*, **217**, 358.
Schneider, D. P., and Young, P. 1980, *Ap. J.*, **238**, 946.
Ulrich, M. H., *et al.* 1980, *M.N.R.A.S.*, **192**, 561.
Weymann, R. J., Latham, D., Angel, J. R. P., Green, R. F., Liebert, J. W., Turnshek, D. A., Turnshek, D. E., and Tyson, J. A. 1980, *Nature*, **285**, 641.
Wills, D., and Netzer, H. 1979, *Ap. J.*, **233**, 1.
Young, P., Deverill, R. S., Gunn, J. E., Westphal, J. A., and Kristian, J. 1981, *Ap. J.*, **244**, 723.
Young, P. J., Sargent, W. L. W., Boksenberg, A., Carswell, R. F., and Whelan, J. A. J. 1979, *Ap. J.*, **229**, 891 (Paper I).

A. BOKSENBERG: Department of Physics and Astronomy, University College London, Gower Street, London WC1E 6BT, England

WALLACE L. W. SARGENT: Department of Astronomy 105-24, California Institute of Technology, Pasadena, CA 91125

PETER YOUNG: Deceased